# Multiresponsive Clay-Containing Layer-by-Layer Films

**ARTICLE** *in* ACS NANO · SEPTEMBER 2011

Impact Factor: 12.88 · DOI: 10.1021/nn202812a · Source: PubMed



**3 AUTHORS:**

Aliaksandr Zhuk
Johnson & Johnson, Skillman, US
**10** PUBLICATIONS **176** CITATIONS
SEE PROFILE

Robert Mirza
Stevens Institute of Technology
**1** PUBLICATION **42** CITATIONS
SEE PROFILE

Svetlana Sukhishvili
Stevens Institute of Technology
**134** PUBLICATIONS **4,818** CITATIONS
SEE PROFILE

# Multiresponsive Clay-Containing Layer-by-Layer Films

**Aliaksandr Zhuk, Robert Mirza, and Svetlana Sukhishvili***

Department of Chemistry, Chemical Biology and Biomedical Engineering, Stevens Institute of Technology, Hoboken, New Jersey 07030, United States

**ABSTRACT** We report on polymer/clay layer-by-layer films responsive to multiple stimuli. Temperature- and salt-responsive films were constructed using assembly of poly(*N*-isopropylacrylamide) (PNIPAM) and montmorillonite clay nanosheets. An additional pH response was achieved by depositing and cross-linking hybrid, dual-network PNIPAM/clay/PNIPAM/poly(methacrylic acid) (PMAA) multilayers. Both types of films remained stable in a wide pH range and were highly swollen. For example, PNIPAM/clay films swelled up to ~14.5 times their dry film thickness in low-salt solutions at 25 °C, as shown by laser scanning confocal microscopy. At temperatures higher than PNIPAM's lower critical solution temperature (LCST) of 32 °C, or in 0.3 M $Na_2SO_4$ solutions at room temperature, both PNIPAM/clay and PNIPAM/clay/PNIPAM/PMAA films reversibly deswelled as a result of collapse of PNIPAM chains. Films of both types showed a decrease in permeability to fluorescein-tagged dextrans of various molecular weights. Importantly, film permeability to dextrans was decreased at temperatures above PNIPAM's LCST, and the effect could be reversed by lowering the temperature. Inclusion of PMAA within multilayers provided an additional pH response to film swelling and permeability. Hybrid PNIPAM/clay/PNIPAM/PMAA films showed drastic deswelling at low pH values due to the onset of hydrogen bonding between PNIPAM and PMAA, and the diffusion of 70 kDa dextran through multilayers at acidic pH was completely blocked. These multiresponse features of clay-containing films make them promising candidates for applications in sensing, actuation, and controlled delivery.

**KEYWORDS:** layer-by-layer films · clay−polymer assembly · swelling · dual pH and temperature response · poly(*N*-isopropylacrylamide) · controlled permeability · nanocomposites

Combining clay nanoparticles with polymers is a promising direction for designing materials that merge advantageous properties of both components. Abundant, inexpensive, and environmentally friendly, clay provides significant mechanical property gains, while polymer is responsible for flexibility of the material. Since 1993, when the Toyota research group produced the first polymer/clay material using Nylon-6,[1] significant progress was achieved in a number of material properties, including superior stiffness and toughness, high thermal stability, and enhanced barrier properties.[2−4] Uniqueness of clay results from the high aspect ratio of dispersed clay nanosheets. One nanometer in thickness and tens-to-micrometers in lateral dimension, exfoliated clay nanosheets act as cross-linkers between polymer chains.

Polymer/clay materials were also explored in the hydrated state. Haraguchi developed a novel class of nanocomposite hydrogels synthesized by free-radical polymerization using *N*-isopropylacrylamide or *N*,*N*-dimethylacrylamide in the presence of inorganic clay nanoparticles.[5] These nanocomposite gels were flexible and exhibited advanced mechanical, optical, and swelling/deswelling properties compared to conventional polymer gels. Very recently, Wang *et al.* reported on a similar application of a mixing approach to produce hydrogels moldable into various shapes by mixing clay with positively charged dendritic binders.[6] Noncovalent interactions between clay surface and amino groups of the dendrimer were able to rearrange and to provide self-healing properties to the material. However, random orientation of clay particles within those gels restricts the potential for exploiting material properties such as barrier and separation membrane properties.

Compared to bulk nanocomposites, layer-by-layer (LbL) self-assembled multilayers are materials with ultrafine nanometer-scale structure. The LbL technique, originally introduced by Decher for oppositely charged polymers, has become one of the core areas of growth in the development of constructing nanoscale films, surfaces, and functional materials with highly tunable architectures and properties.[7−13] Clay-containing LbL films composed of negatively charged clay nanoparticles and polycations have been widely studied.[14−17] Electrostatic assembly of polycations with clay nanoparticles is enabled by the presence of negative charges at the clay surface. Montmorillonite, one of the commonly used clay types, is made up of one octahedral alumina sheet sandwiched between two tetrahedral silica sheets. Natural substitution of, approximately, one in six of the aluminum ions in the octahedral layers of montmorillonite by magnesium or other divalent ions results in isomorphism. This

* Address correspondence to ssukhish@stevens.edu.

Received for review July 25, 2011 and accepted September 29, 2011.

**Published online September 29, 2011**
**10.1021/nn202812a**

gives negative charges that are counterbalanced by cations, such as $Na^+$, $K^+$, and $Ca^{2+}$, located in the interlayer (0.5−1.2 electron charges per pseudounit cell, and the corresponding cation exchange capacity is 0.6−1.6 meq $g^{-1}$). Ionic pairing between negatively charged clay nanosheets and positively charged polymer chains occurs due to replacement of charge-compensating $Na^+$ at the clay basal plane by polycation units.[18] In addition to electrostatically assembled polycation/clay LbL films, assembly of clay-containing films can also be driven by secondary interactions. For example, nacre-mimicking layered nanocomposites of clay nanosheets and polyvinyl alcohol (PVA) have been prepared by both one-step[19] and LbL assemblies.[20] Such composites are stabilized by ion−dipole interactions between exchangeable cations and polar polymer segments, as well as by hydrogen-bonding between −OH groups of PVA and $SiO_4$ tetrahedrons in the clay basal plane.[21]

Clay-containing LbL films have mechanical properties superior to their all-polymer counterparts. Clay particles, a few tens of nanometers to several micrometers in length and width, were found to adsorb parallel to the surface, thereby improving film strength and Young's modulus. At the same time, polymer constituents ensure flexibility of the film. As demonstrated with electrostatically assembled polymer/clay, as well as with cross-linked PVA/clay LbL films or assembly of silk fibroin with clay, these layered materials show high Young's modulus and are structurally similar to mussel and oyster shells, known to be one of the toughest natural mineral-based materials.[20,22−24]

Apart from enhanced mechanical properties, LbL clay-containing films show exceptional oxygen-barrier properties, which lie at the heart of their applications as flame-retardant[25,26] or anticorrosion coatings.[27] Electrostatic assemblies of cationic polymers, such as poly(diallyldimethylammonium chloride) (PDDA), polyallylamine hydrochloride, polyethyleneimine (PEI), and poly(2-vinylpyridine) have been used as barrier coatings to prevent diffusion of various gaseous permeants, including water vapors and oxygen.[15,16,28−30] Due to the high aspect ratio and parallel alignment of clay platelets during their assembly, such coatings are very efficient. For example, an ultrathin (∼50 nm thick), layered clay-containing coating reduced the oxygen diffusion rate below the detection limit.[30] However, the potential of clay-containing multilayers as membranes for filtration and separation of molecules in solution has not yet been explored. Except for one known to us example of the use of polymer/clay LbL coatings to control permeability of methanol through a Nafion membrane for fuel cell applications,[31] other reports on the use of LbL membranes to control permeability of solutes in aqueous solutions involve all-polymer LbL films.

Here, we constructed temperature-responsive clay-containing LbL films by using poly(*N*-isopropylacrylamide) (PNIPAM) as a building block in film assembly and explored their stimuli-response properties in an aqueous environment. Additional pH response was achieved by incorporation of a third component—a weak polyacid—within LbL assemblies. Using confocal microscopy and *in situ* phase-modulated ellipsometry, we revealed the multiresponsive swelling properties of clay-containing assemblies and their ability to control permeability of solutes of various molecular weights in response to environmental stimuli. As compared to earlier reported all-polymer temperature-responsive LbL films,[32−34] inclusion of clay within multiply responsive LbL films enhances mechanical robustness of the films, while maintaining inherent temperature, pH, and salt response supported by polymer film components. Such organic−inorganic nanocomposites might find applications in sensing, actuation, and separation technologies.

## RESULTS AND DISCUSSION

**PNIPAM/Clay Multilayers.** We first demonstrated deposition of LbL nanofilms by assembly of montmorillonite clay nanosheets with two different neutral polymers: temperature-responsive PNIPAM or PVPON, which does not show temperature sensitivity in aqueous environments and was used as a control. Electrostatically assembled films of PEI and clay nanosheets were used as another control. Optimized deposition of clay nanosheets as monolayers within LbL films occurred after 6−7 min deposition from 0.2 mg/mL solutions. Figure 1 and Figure S1 in the Supporting Information show film thickness measurements, obtained with ellipsometry and atomic force microscopy (AFM) for PNIPAM/clay and PVPON/clay films, respectively. In both cases, film thickness increased in a linear fashion as a function of bilayer number, with 4.6 ± 0.2 and 4.1 ± 0.1 nm deposited per bilayer in the case of PNIPAM/clay and PVPON/clay systems, respectively. In the case of PEI/clay multilayers, thickness per bilayer was 3.5 nm (data not shown), in good agreement with earlier reports for electrostatic polymer/clay assemblies.[15,28] An AFM image (Figure 1B) indicates surface morphology of a three-bilayer PNIPAM/clay film, with a typical root-mean-square roughness of 1.8 nm. SEM analysis of a cross section of a 400-bilayer film (Figure 1C and 1D) revealed a thickness of 1.85 ± 0.05 $\mu$m, suggesting a deposition of ∼4.6 nm per bilayer, in good agreement with ellipsometry and AFM data. Importantly, unlike hydrogen-bonded PNIPAM/polycarboxylic acid LbL films,[35] PNIPAM/clay assemblies showed exceptional pH stability. Multilayers could be deposited in the pH range from 3 to 10 and did not disintegrate upon pH variations. The mechanism of binding of neutral polymers to clay nanosheets might be similar to that suggested for binding of polar organic molecules with clay particles.[21,36] We suggest that the mechanism includes a combination of van der Waals and

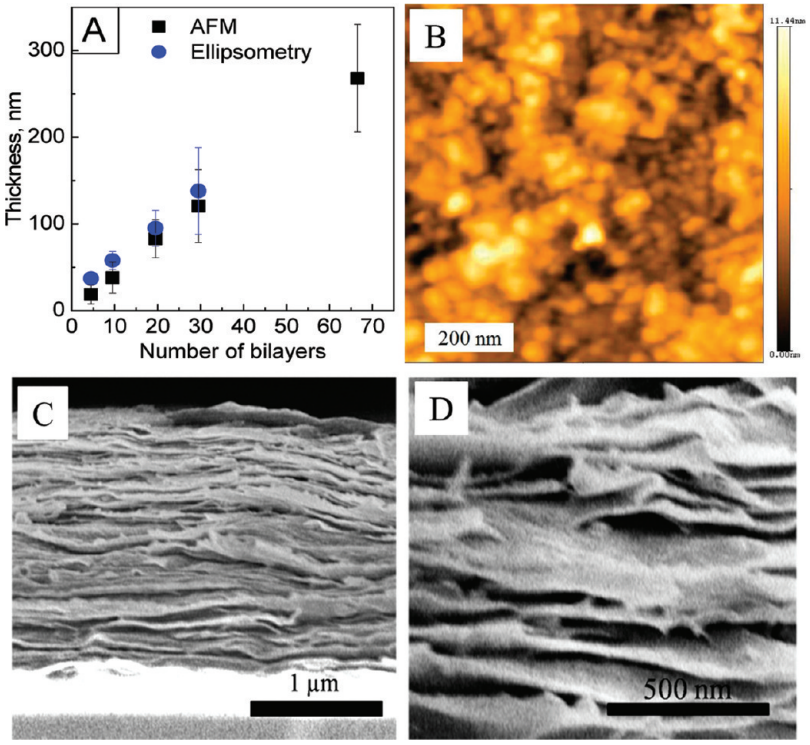


**Figure 1. (A) Ellipsometry (circles) and AFM (squares) dry thicknesses of PNIPAM/clay self-assembly as a function of bilayer number; (B) AFM images of dry $(PNIPAM/clay)_3$ film deposited at a silicon wafer (scanned area of 0.8 $\mu$m), showing a root-mean-square AFM roughness of 1.8 nm; (C and D) SEM images of cross section of a 400-bilayer PNIPAM/clay LbL film. All films were deposited from 0.01 M phosphate buffer solutions at pH 6.5 and 25 °C.**

dipole−cation interactions between the polymer and the clay basal plane. Binding of PNIPAM or PVPON with clay edges is less likely, since film growth did not correlate with the charge state of functional groups at the clay edges ($pK_a$ of AlOH and SiOH groups ~6−7).[37]

In order to investigate the ability of PNIPAM/clay multilayers to swell/deswell with temperature changes, we carried out an *in situ* confocal laser scanning microscopy (CLSM) study. CLSM images of a cross-section of $(PNIPAM/clay)_{400}$ films in 0.01 M phosphate buffer at pH 7.5 and 25 °C (Figure 2, Table 1) showed that multilayers reversibly take up a large amount of water, swelling 14.5 times their dry thickness (*i.e.*, to 25.6 ± 1.20 $\mu$m from 1.8 ± 0.1 $\mu$m in dry films). Such a high swelling ratio can be explained by a relatively low number of binding sites between PNIPAM's amide groups and clay's basal surface. Studies of swelling kinetics demonstrated that the swelling ratio of PNIPAM/clay reached its equilibrium value in 30 min at 25 °C (Figure S2). Such a slow swelling is probably due to the large number of bilayers deposited within a film, as well as due to significant constraints associated with steric restrictions on repositioning of the asymmetric clay nanosheets within highly swollen PNIPAM/clay hydrogels.

A CLSM image of the $(PNIPAM/clay)_{400}$ system shows that raising the temperature above PNIPAM's LCST of ~32 °C[35] or the use of the 0.3 M $Na_2SO_4$ solution at 25 °C both result in a significant film deswelling (~40% compared to film thickness in a low-salt solution at 25 °C). Importantly, film swelling/deswelling in response to both temperature and salt variations were fully reversible and could be repeated at least four times. In both cases, film deswelling results from collapse of PNIPAM chains. In salt solutions, LCST of PNIPAM is decreased due to binding of anions with PNIPAM polymer chains, as suggested by the Hofmeister series. In 0.3 M $Na_2SO_4$ solutions, for example, LCST of PNIPAM is decreased to 24 °C,[38] resulting in PNIPAM/clay films collapsing in 25 °C solutions (Figure 2, Table 1).

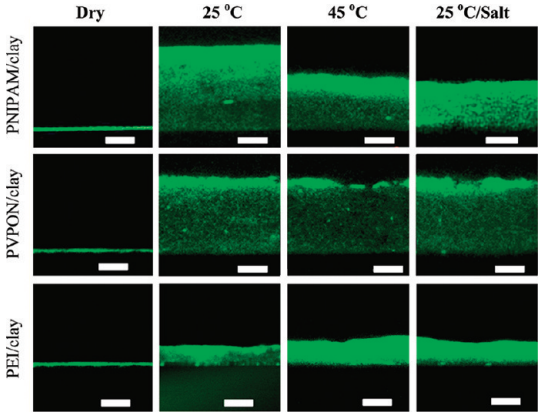


**Figure 2. CLSM images of a cross-section of $(polymer/clay)_{400}$ films deposited on a Si wafer. Left-to-right: dry film; swollen film at 25 °C in 0.01 M phosphate buffer at pH 7.5; in phosphate buffer of pH 7.5 at 45 °C; and in 0.3 M $Na_2SO_4$ at 25 °C. The scale bar is 10 $\mu$m.**

**TABLE 1. Comparison of CLSM Results for 400-Bilayer PNIPAM/Clay, PVPON/Clay, and PEI/Clay Films[a]**

| | thickness ($\mu$m)[b]/swelling ratio | | | |
|---|---|---|---|---|
| | dry | wet, 25 °C, no salt | wet, 45 °C, no salt | wet, 45 °C, 0.3 M $Na_2SO_4$ |
| $(PNIPAM/clay)_{400}$ | 1.8/1 | 26.1/14.5 | 16.1/8.9 | 15.3/8.5 |
| $(PVPON/clay)_{400}$ | 1.8/1 | 25.6/14.3 | 25.1/14.0 | 25.4/14.2 |
| $(PEI/clay)_{400}$ | 1.7/1 | 7.4/4.4 | 8.1/4.8 | 9.1/5.4 |

[a] Measurements of film swelling were performed in 0.01 M phosphate buffer solutions at pH 7.5 with or without additional salt. Prior to *in situ* measurements, films were kept for 30 min in corresponding solutions to reach equilibrium swelling. [b] Errors of thickness measurements were within 8%.

Interestingly, while in buffer and salt-containing solutions, PNIPAM/clay films were relatively smooth at the micrometer scale at temperatures both below and above PNIPAM's LCST (Figure 2), the films exposed to 45 °C in salt-free solutions (DI water at pH 5.6) had a buckled morphology (Figure S3). Such buckling results from the "card-house" effect when edges of a clay nanosheet (*i.e.*, edge Al−OH, Si−OH, Mg−OH, and Fe−OH groups) stick to the basal plane of surrounding clay nanosheets[39] during temperature- or salt-triggered film deswelling. In salt-free solutions, contacts between clay nanosheets in the collapsed "card-house" do not rearrange, resulting in film buckling and also in strong mechanical stress at the film−substrate interface. In these conditions, PNIPAM/clay films could be harvested from the substrate by simply cycling the temperature of the immersion solution above and below PNIPAM's LCST (Figure S3). At the same time, in buffer and salt-containing solutions with significant electrostatic screening, bonds could be rearranged within the film and contact cured, resulting in smooth film surfaces seen in Figure 2. Correspondingly, film temperature cycling did not result in facile film delamination.

Control experiments with PVPON/clay and PEI/clay films deposited onto silicon substrates showed that those films showed no temperature and/or salt response (Figure 2). The data on swelling of these control systems, along with swelling of PNIPAM/clay films, are summarized in Table 1. Interestingly, swelling ratios of assemblies of neutral polymers (PNIPAM/clay at 25 °C and PVPON/clay) were much higher than those of the assembly of a cationic polymer (PEI/clay) (~14 *versus* ~4.5, respectively). This drastically different swelling behavior is due to differences in binding mechanisms between these polymers. Moderate swelling of a cationic PEI with clay nanosheets is a result of strong "zip-lock" binding of a polycation with negative sites at the basal planes of clay nanosheets. Unlike cationic polymers, PNIPAM and PVPON bind with clay through weaker dispersive interactions and tend to adsorb at the clay surface in a loopier, closer-to-random-coil conformation. Swelling behavior and temperature response of clay-containing PNIPAM/clay multilayers have been additionally studied by *in situ* ellipsometry. These results are discussed in the Supporting Information. Figure S4 shows that ellipsometrically measured deswelling of $(PNIPAM/clay)_5$ film caused by immersion in pH 7.5 0.3 M $Na_2SO_4$ solutions at 25 °C showed trends similar to those revealed in CLSM studies.

We then sought to explore the permeability of PNIPAM/clay assemblies in aqueous solutions and their dependence on temperature and salt concentration. After depositing 10 bilayers of PNIPAM/clay at the surface of 100-nm-pore-size polycarbonate membranes, the pores became fully covered. With an example of a 60-bilayer PNIPAM/clay film, Figure S5 shows that the multilayer coating did not change morphologically and the pores remained covered after the permeability runs. Figure 3 summarizes the data on permeability of a multilayer-coated membrane to a fluorescent dye, fluorescein-5-isothiocyanate (FITC), and fluorescently tagged dextrans (FITC-dextrans) of various molecular weights. All permeability studies were performed with $10^{-4}$ mg/mL of permeant in 0.01 M phosphate buffer at pH 7.5. Figure 3A illustrates that the permeability factor, $P$, showed little dependence on the number of bilayers in PNIPAM/clay films for a low molecular weight molecule, *e.g.*, FITC, reducing its permeability factor by only ~60% (from $P = 3.24 \times 10^{-4}$ cm/s for bare polycarbonate membrane to $P = 1.41 \times 10^{-4}$ cm/s for the membrane with 60 bilayers of PNIPAM/clay). Because of the large degree of swelling of the PNIPAM/clay system, multilayers did not provide any significant permeability barrier for a small molecule. It is likely that a modest decrease in permeability of FITC molecules is determined by only the first few layers of PNIPAM/clay. A similarly small effect of reduction of small molecule permeability was reported for diffusion of methanol from a 50/50 water/methanol mixture through $(polyacetylene/clay)_{20}$ film.[31] This suggestion is reasonable, considering that the closest-to-the substrate clay layer, covering approximately 60−90% of the surface, is tightly attached to the PEI precursor layer.[28] In contrast, the effect of PNIPAM/clay LbL films on permeability of FITC-dextrans with molecular weights of 4, 70, 150, and 500 kDa was much stronger (Figure 3A and B). This can be rationalized considering an increase on dextran hydrodynamic radius from 3 nm for 4 kDa molecular weight dextran to 12, 13, and 16 nm for 70, 150, and 500 kDa, respectively.[40,41] The effect of molecular weight of FITC-dextrans was strong, with the permeability factor, $P$, for 500 kDa FITC-dextran reduced from $2.02 \times 10^{-5}$ cm/s for bare polycarbonate membrane to $1.08 \times 10^{-7}$ cm/s for its diffusion through $(PNIPAM/clay)_{60}$ film (99.5% reduction). The diffusion coefficients for permeation of solutes through PNIPAM/clay multilayers calculated as $D = Pd$, where $d$ is the membrane

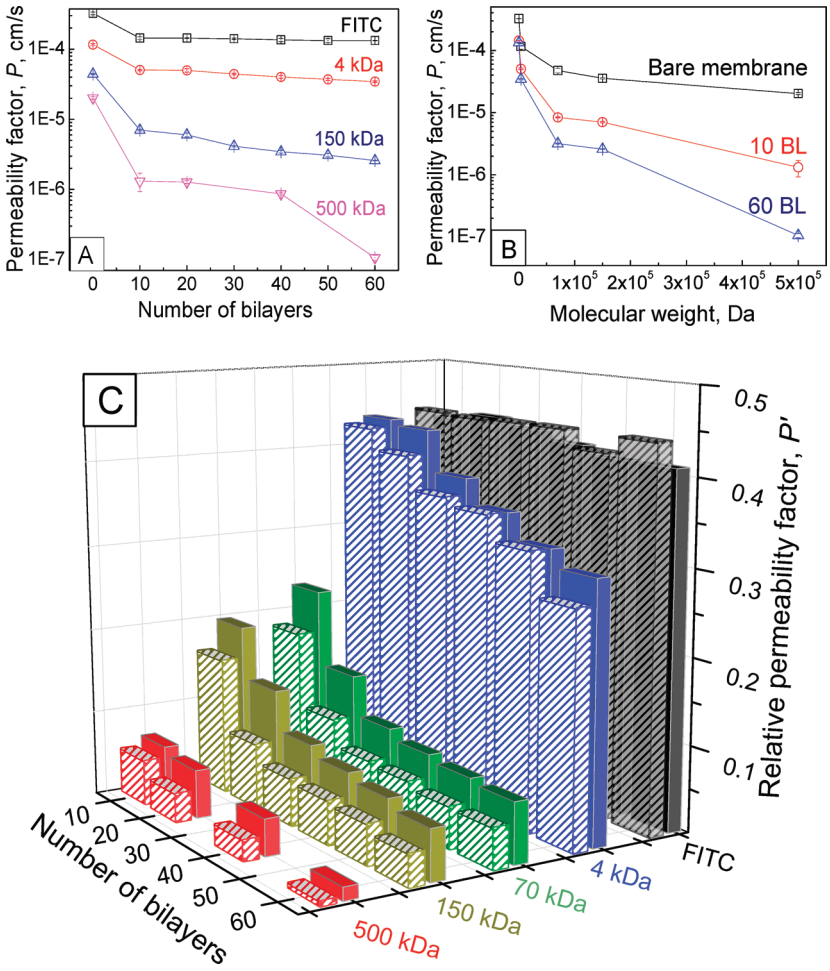


**Figure 3. Permeability of PNIPAM/clay multilayers to FITC and FITC-labeled dextrans of various molecular weights: effect of film thickness and molecular weight of a permeant in measurements at 25 °C (A and B, respectively), as well as the effect of temperature on solute permeability (C). In (C), solid bars represent measurements at 25 °C and patterned bars, those at 45 °C. All experiments are performed in 0.01 M phosphate buffer solution at pH 7.5. Multilayers were deposited on a polycarbonate membrane according to the procedure described in the Experimental Section.**

thickness, were $(6 \pm 2) \times 10^{-10}$, $(7 \pm 2) \times 10^{-11}$, $(6 \pm 1) \times 10^{-11}$, and $(9 \pm 4) \times 10^{-12}$ cm$^2$/s for FITC-dextrans with molecular weights of 4, 70, 150, and 500 kDa, respectively. These values are at least 3 orders of magnitude lower than diffusion coefficients of corresponding molecules in solution ($D$ of $7.2 \times 10^{-7}$, $1.8 \times 10^{-7}$, $1.63 \times 10^{-7}$, and $1.3 \times 10^{-7}$ cm$^2$/s have been calculated using the Stokes–Einstein equation based on hydrodynamic sizes of 4, 70, 150, and 500 kDa, respectively).

Figure 3C also shows the effects of temperature on permeability of PNIPAM/clay multilayers to various solutes. In Figure 3C, the data are presented as the relative permeability factor, $P'$, calculated as a ratio of permeability factors of films deposited on the membrane to the permeability of the bare membrane at corresponding temperatures. Temperature-induced deswelling of PNIPAM/clay multilayers shown in Figure 2 and Table 1 had an effect on film permeability to various solutes, and the effect was dependent on the solute molecular weight. For a small organic molecule, FITC, the permeability factor showed no dependence on temperature, confirming our suggestion that its permeability is, probably, controlled by clay layers adjacent to the supporting membrane. The temperature dependence of $P'$ was also weak for an oligomeric FITC-dextran with a molecular weight of 4 kDa, suggesting that the temperature-induced film shrinkage does not significantly affect its mesh size in the range ~1–2 nm. For dextrans with molecular weights 70 kDa and higher, the permeability factors decreased ~1.5 times at 45 °C from its value at 25 °C for multilayers of various thicknesses. These data suggest that changes in a film's ~10–20 nm mesh size occur during deswelling that significantly affect film permeability to macromolecules. Scheme 1 shows possible structural changes occurring within PNIPAM/clay films during swelling/deswelling. When PNIPAM/clay films swell, the interlayer distance between clay particles is much larger than hydrodynamic sizes of all studied dextran molecules. It is feasible that molecular permeability is only affected by the distance between clay nanosheets

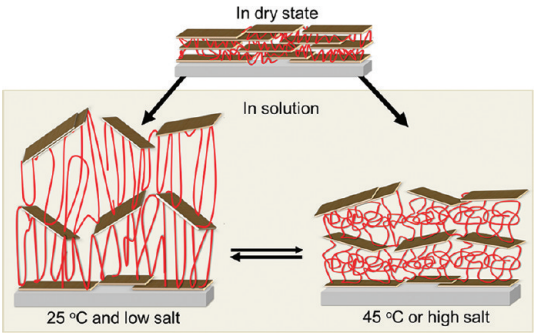


**Scheme 1. Schematic representation of suggested temperature or salt effects on (PNIPAM/clay)$_n$ swelling.**

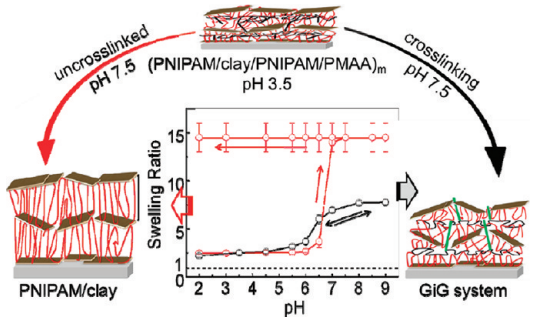


**Figure 4. *In situ* ellipsometry profiles for (PNIPAM/clay/PNIPAM/PMAA)$_3$ un-cross-linked films (red, open circles) and the same films, cross-linked in 3 mg/mL solutions of ethylenediamine and CDI for 2.3 h (black, filled circles). Starting from acidic pHs, films were exposed to 0.01 M phosphate buffers with increasing pH values for 15 min. After measurements at pH 9, buffer pH was gradually lowered. Dashed line indicates dry film.**

within a single layer, which decreases as PNIPAM/clay films deswell. An alternative explanation is that at higher temperatures dextran molecules diffuse through a tighter mesh of PNIPAM loops.

**Dually Responsive Gel-in-Gel (GiG) LbL Films.** We then aimed to endow temperature-responsive PNIPAM/clay LbL assemblies with additional pH response properties. This was achieved by replacing every other clay layer during assembly with poly(methacrylic acid) (PMAA). Film assembly was performed at acidic pH values to ensure hydrogen bonding between the protonated form of PMAA and PNIPAM[10] and resulted in (PNIPAM/clay/PNIPAM/PMAA)$_m$ films, where $m$ is the number of deposited quadrolayers, QLs. Multilayer growth was linear, with a 19 $\pm$ 2 nm dry thickness per QL. This value is ~10 nm higher compared to a 9 nm thickness for two PNIPAM/clay bilayers. After film deposition, assembled PMAA was selectively cross-linked within the films through its carboxylic groups using carbodiimide (CDI) chemistry and ethylenediamine as a cross-linker. This procedure has been established earlier in our group for cross-linking of all-polymer, PMAA-containing hydrogen-bonded multilayers.[42] Clay-containing 3-QL films were then exposed to 0.01 M phosphate buffer solutions at pH 7.5 for 30 min. Un-cross-linked

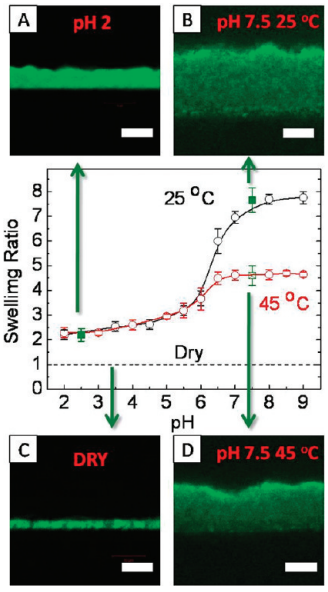


**Figure 5. Swelling ratios of m-QL GIG films at 25 °C (black) and 45 °C (red) as measured by ellipsometry (circles) and CLSM (squares); $m$ is equal to 3 and 200 in *in situ* ellipsometry and CLSM studies, respectively. From A to D: corresponding CLSM images of a cross-section of a 200-QL GiG film deposited at the surface of Si wafers in 0.01 M phosphate buffer at pH 2 and 25 °C (A); in the dry state (C); or free-floating films in pH 7.5 solutions at 25 °C (B) or 45 °C (D). Multilayers were deposited at pH 3.5 and cross-linked for 2.3 h. The scale bar is 10 $\mu$m.**

multilayers showed a loss of ~35% dry film mass as indicated by ellipsometry measurements of dry films (for example, for 3-QL film, dry thickness decreased from 60 to 40 nm). Films cross-linked for 2.3 h or longer time showed no changes in dry thickness after pH cycling between 2 and 9, and 1-h-cross-linked films presented the intermediate case, showing partial loss of PMAA due to incomplete polyacid cross-linking (corresponding to ~25–30% dry thickness reduction).

Figure 4 compares swelling behavior of cross-linked and un-cross-linked 3-QL films. Without cross-linking, films release hydrogen-bonded PMAA when exposed to pH 7.5, while PNIPAM is retained within the film due to binding with clay nanosheets. When pH is subsequently cycled between basic and acidic values, these films lose their pH responsiveness and behave similarly to PNIPAM/clay system, showing a high swelling ratio of ~14.5. This suggests that PMAA was completely released from un-cross-linked 3-QL films. In drastic contrast, 2.3-h-cross-linked 3-QL films swell to a smaller degree when exposed to high pHs and show fully reversible, pH-dependent swelling. Herein, we denote these cross-linked structures as gel-in-gel (GiG) structures, where "first gel" refers to covalently cross-linked PMAA (PMAA-gel) and "second gel" refers to highly swollen PNIPAM/clay multilayers. Since PMAA molecules are cross-linked "through" clay layers, such GiG structures consist of two interpenetrated networks. At acidic pH, cross-linked PMAA network is strongly

hydrogen-bonded to clay-bound PNIPAM, showing a low swelling ratio of ~2. An increase in pH above $pK_a$ of PMAA (~6.4[35]) results in dissociation of hydrogen bonds between PMAA and PNIPAM and enhances film swelling. At high pH values, PNIPAM remains bound to clay nanosheets, and the entire network swells up to ~8 times its dry thickness as a result of electrostatic expansion of the PMAA network and high swelling propensity of the PNIPAM/clay matrix. As compared to PNIPAM/clay multilayers, a lower swelling ratio for GiG systems (swelling ratios 14.5 and 8, respectively) is probably due to restrictions imposed by PMAA gel to swelling of the PNIPAM/clay network.

Dual response of 2.3-h-cross-linked GiG films to pH and temperature was further investigated using *in situ* CLSM and ellipsometry. Figure 5 shows that both techniques gave consistent results. For *in situ* ellipsometry, 3-QL GiG films with a dry thickness of 51 nm were used. For CLSM studies, 200-QL GiG films (of 2.9 ± 0.2 μm dry thickness) were deposited at the surface of Si wafers. Figure 5A and B show CLSM images of a 200-QL GiG film cross-section at low and high pH values at 25 °C. Interestingly, at basic pH values, GiG films retained its temperature response as PNIPAM chains were dissociated from the PMAA network (Figure 5). At temperatures above 32 °C, the swelling ratio of GiG systems decreased by ~40% as a result of temperature-induced collapse of PNIPAM chains.

The amplitude of film swelling and its pH and temperature responses could be controlled by the cross-linking density of the PMAA gel, varied with exposure time to cross-linking solutions. Figure 6 summarizes *in situ* ellipsometry swelling results for 3-QL GiG films cross-linked for 2.3 to 8 h and exposed to pH 7.5. An increase in cross-linking time results in an increase in number of cross-links between PMAA chains and in reduction of film swelling. Along with a decrease in the amplitude of film pH response, temperature effects on film swelling also weakened for highly cross-linked films (Figure 6 and S6). An 8-h-cross-linked 3-QL GiG film completely lost its ability to respond to pH and temperature variations. In these highly cross-linked double-network hydrogels, the tightly cross-linked PMAA network restricts changes in PNIPAM/clay network swelling.

Importantly, GiG films strongly reduced permeability of various solutes. Unlike PNIPAM/clay films (see Figure 3), 5-QL GiG multilayers with a dry thickness of ~90 nm deposited on polycarbonate membrane reduced the permeability of FITC ~70-fold at 25 °C as compared to bare membrane (data not shown). Figure 7 shows barrier properties of 5-QL GiG films to permeation of 70 kDa FITC-dextran. At pH 7.5, the relative permeability factor, $P'$, of ~0.008 was achieved (as compared to $P'$ of ~0.23 for 10-bilayer PNIPAM/clay films), and, in contrast to the PNIPAM/clay system, permeability could be further controlled by pH variations (Figure 7A). In particular, a decrease in pH to 3 for GiG membrane reestablished hydrogen bonding

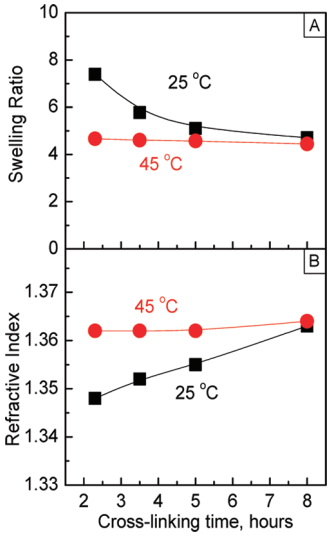


**Figure 6. Effect of cross-linking time on swelling of 3-QL GiG films at pH 7.5 and 25 °C (circles) and 45 °C (squares) as measured by *in situ* ellipsometry.**

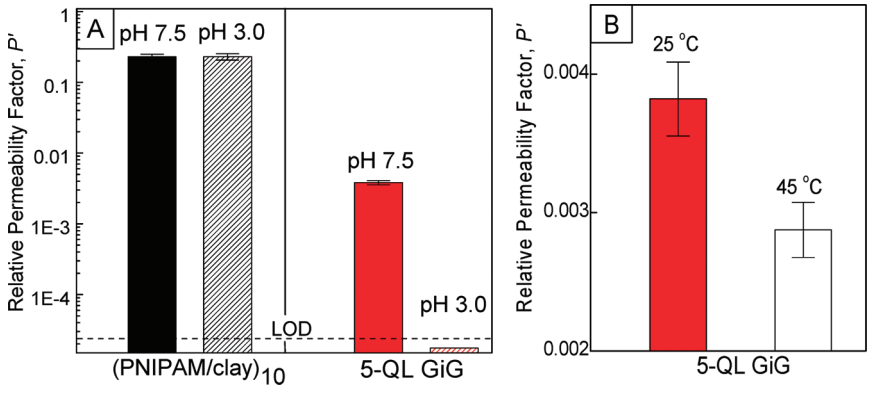


**Figure 7. (A) Effect of pH on permeability of $(PNIPAM/clay)_{10}$ and 2.3-h-cross-linked 5-QL GiG films (dry thicknesses ~45 and ~90 nm, respectively) to 70 kDa FITC-dextran at 25 °C and (B) effect of temperature on permeability of 5-QL GiG films to 70 kDa FITC-dextran in 0.01 phosphate buffer solution at pH 7.5. Dashed line in panel A shows the limit of detection (LOD) of permeability measurements. Permeability of a 5-QL GiG film at pH 3.0 was below the detectable value.**

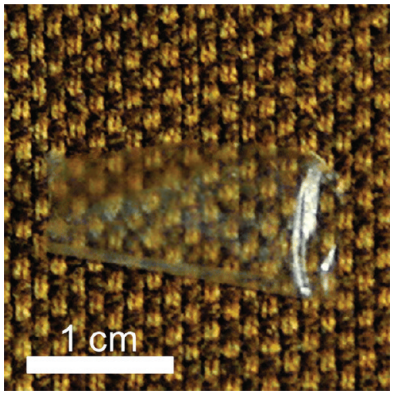


**Figure 8. Digital photograph of dry, ~3.5-$\mu$m-thick, free-standing 200-QL GiG film released from a Si wafer by exposure to 0.01 M phosphate buffer solutions at pH 7.5.**

between PNIPAM and cross-linked PMAA chains, reducing the permeability of the film to 70 kDa FITC-dextran molecules below the detection limit indicated in Figure 7A. Figure 7B shows that permeability of GiG films to FITC-dextrans was responsive to temperature, in correlation with temperature-induced changes in film swelling. Importantly, effects of pH and temperature on film permeability were fully reversible.

Finally, while thinner GiG films used for *in situ* ellipsometry and permeability experiments remained attached to the substrates, thicker films with the number of QLs above ~50 were easily detached from substrates by immersing them in solutions at 25 °C with pH > 7. In these conditions, drastic film swelling (see Figure 6) resulted in strong mechanical stress at the film/substrate interface, leading to film delamination. Our results suggest that with films composed of less than 50 QL, such mechanical stress was not sufficient to disrupt strong binding between oxidized silicon surface, PEI precursor, and closest-to-the-substrate clay layer. Compared to PNIPAM/clay films, GIG films were easier to handle in both their wet and dry state. Figure 8 shows that delaminated films remained highly transparent. As revealed by UV−vis spectroscopy (Figure S7), 3.6-$\mu$m-thick, 200-QL GiG film transmitted >90% of incident light in a wide spectral region between 240 and 1000 nm. Unlike other reported approaches to release LbL films from substrates, this technique does not require the use of organic solvents,[43] extreme pH, high salt concentrations,[44] temperature variations,[34] or the use of sacrificial layers.[34,45]

In summary, here we reported on polymer/clay LbL assemblies that respond to temperature, pH, and salt concentration variations *via* changes in their swelling ratio and permeability characteristics to various solutes. Unlike previous studies of polymer/clay LbL films preformed with dry multilayers,[16,17,30] these multilayers operate in aqueous environment. The multilayer permeability to dextran molecules was selective to solute molecular weights and could be further controlled by pH and/or temperature stimuli. Importantly, inclusion of clay nanosheets within responsive films enhanced mechanical robustness of the films as compared to their all-polymer counterparts. These robust "smart" materials are promising candidates for a variety of applications,[46] ranging from tissue engineering to biosensing and bioseparation. As substrate-attached or free-standing films, these assemblies might be useful for controlling flow, diffusion, and adhesion in confined environments including microfluidic and biomedical devices.

## EXPERIMENTAL SECTION

**Materials.** Poly(*N*-isopropylacrylamide) ($M_w$ 300 kDa) and poly(methacrylic acid) ($M_w$ 150 kDa) were purchased from Scientific Polymer Products Inc. Poly(*N*-vinylpyrrolidone) (PVPON; $M_w$ of 55 kDa), poly(ethyleneimine) ($M_w$ 600 kDa), fluorescein isothiocyanate dextran (FITC-dextran; $M_w$ of 4, 70, 150, and 500 kDa) hydrochloric acid, sodium hydroxide, sodium chloride, and dibasic and monobasic sodium phosphate were purchased from Sigma-Aldrich Inc. Fluorescein-5-isothiocyanate and Alexa Fluor 488 hydrazide, sodium salt, were obtained from Molecular Probes, Inc. All chemicals were used without further purification. $Na^+$-Montmorillonite clay (Cloisite-$Na^+$) was donated by Southern Clay Products (Gonzales, TX). Clay dispersions were prepared by dissolving 5 g of clay in deionized water (DI water) under vigorous stirring for 1 day, allowing larger particles to precipitate at the bottom of the container overnight, and collecting supernatant solution. The supernatant solution was diluted 10 times and used for film deposition. The $H_2O$ used in all experiments was deionized and further purified by passage through a Milli-Q System (Millipore). Unless otherwise noted, 0.01 M phosphate buffer solutions were used to control pH. The silicon wafers were prime grade, p-type with boron dopant, 525 ± 25 $\mu$m thick, with a native grown oxide layer of ~20 Å and were purchased from Cemat Silicon S.A. and cut with a Fletcher steel wheel glass cutter.

**Deposition of Multilayers.** Multilayers were deposited at the surface of oxidized Si wafers. Prior to film deposition, silicon wafers were irradiated with UV light for 2 h to remove organic impurities from the surface of supplied wafers, followed by washing with DI water and treating with concentrated sulfuric acid for 10 min. After rinsing with DI water, the silicon wafers were immersed in 0.25 M NaOH solution for 10 min, rinsed with DI water, and dried under a flow of nitrogen. A layer of PEI was deposited as a precursor film to increase the surface adhesion of clay particles to the substrate. To deposit the precursor layer, cleaned silicon wafers were first exposed to 0.2 mg/mL PEI solution at pH 6.5 for 15 min and then rinsed with phosphate buffer solution at the same pH.

Film deposition was performed by alternating immersion of silicon wafer in solutions of clay for 6 min and polymer for 15 min starting with clay. After deposition of each polymer, the wafers were rinsed in two buffer solutions for 1 min each. Deposition was performed from 0.2 mg/mL polymer solutions in 0.01 M phosphate buffer at pH 6.5. For rinsing steps, 0.01 M phosphate buffer with the same pH was used. The Robot Arm Catalyst 3 (CRS Robotics Corp.) system operated with homemade software was used for multilayer construction. The pH values of buffer

solutions were adjusted using 0.01 M HCl or 0.01 M NaOH solutions. For gel-in-gel films, every other clay layer was replaced with PMAA. Deposition was performed from 0.2 mg/mL solutions at pH 3.5. After deposition of multilayers cross-linking was performed by activation of carboxylic groups with 3 mg/mL of 1-ethyl-3-(3-(dimethylamino)propyl)carbodiimide hydrochloride solution at pH 5.0 for 20 min, followed by reacting with 3 mg/mL of ethylenediamine at the same pH for various time.

**Ellipsometry Measurements.** Film thickness measurements were performed using a home-built single-wavelength phase-modulated ellipsometer at 65° and 70° angles of incidence for dry and wet measurement, respectively. Detailed description of the ellipsometry setup and swelling measurements can be found in other publications.[47] The optical properties of the silicon substrates and oxide layer thickness were determined prior to polymer deposition. Prior to ellipsometry measurements, all films were blow-dried with nitrogen gas. For measurement of dry films, the refractive index of all polymer films was fixed at 1.5. Studies of film swelling were performed using a cylindrical flow through a temperature-controlled liquid cell. The silicon substrate was placed in an ellipsometry cell, which was then filled with buffer solution with adjusted pH and salt concentration. Measurements were performed after the temperature was allowed to equilibrate for 30 min.

**Atomic Force Microscopy.** AFM measurements were performed in air at room temperature using a NSCRIPTOR dip pen nanolithography system, Nanoink. The instrument was operated in the ac (tapping) mode using P-MAN-SICC-0 AFM cantilevers (Pacific Nanotechnology, Inc.) with a nominal force constant of 40 N/m. A prior thickness measurement step was made with the razor.

**SEM.** SEM images were obtained using an Auriga scanning electron microscope. Si wafers or polycarbonate membranes were attached to the SEM stage using conductive tape. A few monolayers of Au–Pt were sputtered onto the sample surface using an RF-plasma chamber with a sputtering time of 10 s. The applied voltage was varied from 1 to 3 kV.

**Confocal Laser Scanning Microscopy.** Confocal images of polymer/clay multilayers were obtained with a CLSM 5 PASCAL laser scanning microscope (Zeiss, Germany) equipped with a C-Apochromat 60×/1.4 water immersion objective. Images were taken using a homemade temperature-controlled cell, where samples were placed vertically in order to be aligned parallel to the laser beam. Thick films containing 400 bilayers were deposited on a Si wafer and cut into 3 by 10 mm samples. Prior to measurements, multilayer films were immersed in a solution of Alexa-488 (excitation wavelength of 488 nm). The dye was adsorbed within the polymer/clay multilayers, allowing film visualization in CLSM experiments. The average thicknesses and standard deviations were determined from 50 measurements over the area of one square millimeter.

**UV–Vis Spectrometry.** UV measurements were performed using a Perkin-Elmer Lambda 40 spectrophotometer.

**Permeability Studies.** In order to investigate permeation through clay-containing films in solution, multilayers were deposited on a polycarbonate substrate. Permeability studies were performed using PermeGear diffusion cells, which included donor and receptor reservoirs equipped with a magnetic stirrer (600 rpm) to provide sufficient intermixing of solution in the cells. The temperature was controlled using a water jacket around the cells. A polycarbonate membrane (nuclepore track-etch membrane with a pore size of 100 nm, Whatman) with deposited multilayer film was placed between half-cells. The donor and receptor cells were filled with $10^{-4}$ M solution of fluorescently active molecules and buffer, respectively.

Periodically, an aliquot of 0.5 mL was taken and analyzed using an RF-1501 Shimadzu spectrofluorometer as a function of time. The permeability factor, $P$ [cm/s], of a permeant across the multilayers determined as an increase of fluorescence intensity over time interval was calculated as

$$P = \frac{I}{I_o}\frac{V}{At}$$

were $I_o$ and $I$ are initial solution fluorescence intensity in donor and receptor cells at time $t$, respectively, $V$ is the volume of the cell (3.4 mL), and $A$ is an effective area of permeation. Relative permeability factor, $P'$, was calculated as a ratio of permeability factors of films deposited on the membrane to those measured with the bare membrane at corresponding temperatures.

*Acknowledgment.* This work was supported in part by the National Science Foundation under Awards DGE-0742462 and DMR-0906474.

*Supporting Information Available:* Ellipsometry and AFM analysis of PVPON/clay film thicknesses; additional ellipsometry, SEM, CLSM, and UV–vis characterization of PNIPAM/clay and 3-QL GiG films. This material is available free of charge *via* the Internet at http://pubs.acs.org.

## REFERENCES AND NOTES


1. Usuki, A.; Kojima, Y.; Kawasumi, M.; Okada, A.; Fukushima, Y.; Kurauchi, T.; Kamigaito, O. Synthesis of Nylon 6-Clay Hybrid. *J. Mater. Res.* **1993**, *8*, 1179–1184.
2. Alexandre, M.; Dubois, P. Polymer-layered Silicate Nanocomposites: Preparation, Properties and Uses of a New Class of Materials. *Mater. Sci. Eng.: R* **2000**, *28*, 1–63.
3. Ray, S. S.; Okamoto, M. Polymer/Layered Silicate Nanocomposites: a Review from Preparation to Processing. *Prog. Polym. Sci.* **2003**, *28*, 1539–1641.
4. Paul, D. R.; Robeson, L. M. Polymer Nanotechnology: Nanocomposites. *Polymer* **2008**, *49*, 3187–3204.
5. Haraguchi, K.; Takehisa, T. Nanocomposite Hydrogels: A Unique Organic-Inorganic Network Structure with Extraordinary Mechanical, Optical, and Swelling/De-swelling Properties. *Adv. Mater.* **2002**, *14*, 1120–1124.
6. Wang, Q.; Mynar, J. L.; Yoshida, M.; Lee, E.; Lee, M.; Okuro, K.; Kinbara, K.; Aida, T. High-Water-Content Mouldable Hydrogels by Mixing Clay and a Dendritic Molecular Binder. *Nature* **2010**, *463*, 339–343.
7. Decher, G.; Hong, J.-D.; Schmitt, J. Buildup of Ultrathin Multilayer Films by a Self-Assembly Process: III. Consecutively Alternating Adsorption of Anionic and Cationic Polyelectrolytes on Charged Surfaces. *Thin Solid Films* **1992**, *210/211*, 831–835.
8. Decher, G. Fuzzy Nanoassemblies: Toward Layered Polymeric Multicomposites. *Science* **1997**, *277*, 1232–1237.
9. Wang, L. Y.; Wang, Z. Q.; Zhang, X.; Shen, J. C.; Chi, L. F.; Fuchs, H. A New Approach for the Fabrication of an Alternating Multilayer Film of Poly(4-vinylpyridine) and Poly(acrylic acid) Based on Hydrogen Bonding. *Macromol. Rapid Commun.* **1997**, *18*, 509–514.
10. Sukhishvili, S. A.; Granick, S. Layered, Erasable Polymer Multilayers Formed by Hydrogen-bonded Sequential Self-Assembly. *Macromolecules* **2002**, *35*, 301–310.
11. Lavalle, P.; Voegel, J.-C.; Vautier, D.; Senger, B.; Schaaf, P.; Ball, V. Dynamic Aspects of Films Prepared by a Sequential Deposition of Species: Perspectives for Smart and Responsive Materials. *Adv. Mater.* **2011**, *23*, 1191–1221.
12. Podsiadlo, P.; Shim, B. S.; Kotov, N. A. Polymer/Clay and Polymer/Carbon Nanotube Hybrid Organic–Inorganic Multilayered Composites Made by Sequential Layering of Nanometer Scale Films. *Coord. Chem. Rev.* **2009**, *253*, 2835–2851.
13. Hammond, P. T. Form and Function in Multilayer Assembly: New Applications at the Nanoscale. *Adv. Mater.* **2004**, *16*, 1271–1293.
14. Kleinfeld, E. R.; Ferguson, G. S. Stepwise Formation of Multilayered Nanostructural Films from Macromolecular Precursors. *Science* **1994**, *265*, 370–373.
15. Lvov, Y.; Ariga, K.; Ichinose, I.; Kunitake, T. Formation of Ultrathin Multilayer and Hydrated Gel from Montmorillonite and Linear Polycations. *Langmuir* **1996**, *12*, 3038–3044.
16. Kotov, N. A.; Haraszti, T.; Turi, L.; Zavala, G.; Geer, R. E.; Dekany, I.; Fendler, J. H. Mechanism of and Defect Formation in the Self-Assembly of Polymeric Polycation-Montmorillonite Ultrathin Films. *J. Am. Chem. Soc.* **1997**, *119*, 6821–6832.
17. Tang, Z.; Kotov, N. A.; Magonov, S.; Ozturk, B. Nanostructured Artificial Nacre. *Nat. Mater.* **2003**, *2*, 413–418.

18. Brigatti, M. F., Galan, E., Theng, B. K. G. Structure and Mineralogy of the Clay Minerals. In *Handbook of Clay Science*; Bergaya, F., Theng, B. K. G., Lagaly, G., Eds.; Elsevier: New York, 2006; pp 40−44.
19. Walther, A.; Bjurhager, I.; Malho, J.-M.; Pere, J.; Ruokolainen, J.; Berglund, L. A.; Ikkala, O. Large-Area, Lightweight and Thick Biomimetic Composites with Superior Material Properties *via* Fast, Economic, and Green Pathways. *Nano Lett.* **2010**, *10*, 2742–2748.
20. Podsiadlo, P.; Kaushik, A. K.; Arruda, E. M.; Waas, A. M.; Shim, B. S.; Xu, J.; Nandivada, H.; Pumplin, B. G.; Lahann, J.; Ramamoorthy, A.; *et al*. Ultrastrong and Stiff Layered Polymer Nanocomposites. *Science* **2007**, *318*, 80–83.
21. Theng, B. K. G. Uncharged or Non-Ionic Polymers. In *Formation and Properties of Clay-Polymer Complexes*; Elsevier: New York, 1979; pp 65−76.
22. Smith, B. L.; Schäffer, T. E.; Viani, M.; Thompson, J. B.; Frederick, N. A.; Kindt, J.; Belcher, A.; Stucky, G. D.; Morse, D. E.; Hansma, P. K. Molecular Mechanistic Origin of the Toughness of Natural Adhesives, Fibres and Composites. *Nature* **1999**, *399*, 761–763.
23. Jackson, A. P.; Vincent, J. F. V.; Turner, R. M. Aphysical Model of Nacre. *Compos. Sci. Technol.* **1989**, *36*, 255–266.
24. Kharlampieva, E.; Kozlovskaya, V.; Gunawidjaja, R.; Shevchenko, V. V.; Vaia, R.; Naik, R. R.; Kaplan, D. L.; Tsukruk, V. V. Flexible Silk-Inorganic Nanocomposites: from Transparent to Highly Reflective. *Adv. Funct. Mater.* **2010**, *20*, 840–846.
25. Jang, W. S.; Rawson, I.; Grunlan, J. C. Layer-by-Layer Assembly of Thin Film Oxygen Barrier. *Thin Solid Films* **2008**, *516*, 4819–4825.
26. Li, Y.-C.; Schulz, J.; Mannen, S.; Delhom, C.; Condon, B.; Chang, S.; Zammarano, M.; Grunlan, J. C. Flame Retardant Behavior of Polyelectrolyte-Clay Thin Film Assemblies on Cotton Fabric. *ACS Nano* **2010**, *4*, 3325–3337.
27. Kachurina, O.; Knobbe, E.; Metroke, T. L.; Ostrander, J. W.; Kotov, N. A. Corrosion Protection with Synergistic LBL/Ormosil Nanostructured Thin Films. *Int. J. Nanotechnol.* **2004**, *1*, 347–365.
28. Kotov, N. A.; Magonov, S.; Tropsha, E. Layer-by-Layer Self-Assembly of Alumosilicate-Polyelectrolyte Composites: Mechanism of Deposition, Crack Resistance, and Perspectives for Novel Membrane Materials. *Chem. Mater.* **1998**, *10*, 886–895.
29. Yang, Y.-H.; Malek, F. A.; Grunlan, J. C. Influence of Deposition Time on Layer-by-Layer Growth of Clay-based Thin Films. *Ind. Eng. Chem. Res.* **2010**, *49*, 8501–8509.
30. Priolo, M. A.; Gamboa, D.; Holder, K. M.; Grunlan, J. C. Super Gas Barrier of Transparent Polymer-Clay Multilayer Ultrathin Films. *Nano Lett.* **2010**, *10*, 4970–4974.
31. Kim, D. W.; Choi, H.-S.; Lee, C.; Blumstein, A.; Kang, Y. Investigation on Methanol Permeability of Nafion Modified by Self-assembled Clay-Nanocomposite Multilayers. *Electrochem. Acta* **2004**, *50*, 659–662.
32. Zhu, Z.; Sukhishvili, S. A. Temperature-induced Swelling and Small Molecule Release with Hydrogen-Bonded Multilayers of Block Copolymer. Micelles. *ACS Nano* **2009**, *3*, 3595–3605.
33. Xu, L.; Zhu, Z.; Sukhishvili, S. A. Polyelectrolyte Multilayers of Diblock Copolymer Micelles with Temperature-Responsive Cores. *Langmuir* **2011**, *27*, 409–415.
34. Zhuk, A.; Pavlukhina, S.; Sukhishvili, S. A. Hydrogen-bonded Layer-by-Layer Temperature-triggered Release Films. *Langmuir* **2009**, *25*, 14025–14029.
35. Kharlampieva, E.; Sukhishvili, S. A. Hydrogen-bonded Layer-by-Layer Polymer Films. *J. Macromol. Sci., Part C: Polym. Rev.* **2006**, *46*, 377–395.
36. Śequaris, J.-M.; Hild, A.; Narres, H. D.; Schwuger, M. J. Polyvinylpyrrolidone Adsorption on Na-Montmorillonite. Effect of the Polymer Interfacial Conformation on the Colloidal Behavior and Binding of Chemicals. *J. Colloid Interface Sci.* **2000**, *230*, 73–83.
37. Bourg, I. C.; Sposito, G.; Bourg, A. C. M. Modeling the Acid-Base Surface Chemistry of Montmorillonite. *J. Colloid Interface Sci.* **2007**, *312*, 297–310.
38. Zhang, Y.; Furyk, S.; Bergbreiter, D. E.; Cremer, P. S. Specific Ion Effects on the Water Solubility of Macromolecules: PNIPAM and the Hofmeister Series. *J. Am. Chem. Soc.* **2005**, *127*, 14505–14510.
39. Lagaly, G.; Ziesmer, S. Colloid Chemistry of Clay Minerals: The Coagulation of Montmorillonite Dispersions. *Adv. Colloid Interface Sci.* **2003**, *100*, 105–128.
40. Toprak, M. S.; McKenna, B. J.; Waite, J. H.; Stucky, G. D. Control of Size and Permeability of Nanocomposite Microspheres. *Chem. Mater.* **2007**, *19*, 4263–4269.
41. Arstrong, J. K.; Wenby, R. B.; Meiselman, H. J.; Fisher, T. C. The Hydrodynamic Radii of Macromolecules and Their Effect on Red Blood Cell Aggregation. *Biophys. J.* **2004**, *87*, 4259–4270.
42. Kozlovskaya, V.; Kharlampieva, E.; Mansfield, M. L.; Sukhishvili, S. A. Poly(methacrylic acid) Hydrogel Films and Capsules: Response to pH and Ionic Strength, and Encapsulation of Macromolecules. *Chem. Mater.* **2006**, *18*, 328–336.
43. Lin, Y.-H.; Jiang, C.; Xu, J.; Lin, Z.; Tsukruk, V. V. Robust, Fluorescent, and Nanoscale Freestanding Conjugated Films. *Soft Matter* **2007**, *3*, 432–436.
44. Dubas, S. T.; Farhat, T. R.; Schlenoff, J. B. Multiple Membranes from "True" Polyelectrolyte Multilayers. *J. Am. Chem. Soc.* **2001**, *123*, 5368–5369.
45. Ono, S. S.; Decher, G. Preparation of Ultrathin Self-standing Polyelectrolyte Multilayer Membrane at Physiological Conditions Using pH-Responsive Film Segments as Sacrificial Layers. *Nano Lett.* **2006**, *6*, 592–598.
46. Stuart, M. A. C.; Huck, W. T. S.; Genzer, J.; Müller, M.; Ober, C.; Stamm, M.; Sukhorukov, G. B.; Szleifer, I.; Tsukruk, V. V.; Urban, M.; *et al*. Emerging Applications of Stimuli-Responsive Polymer Materials. *Nat. Mater.* **2010**, *9*, 101–113.
47. Pristinski, D.; Kozlovskaya, V.; Sukhishvili, S. A. Determination of Film Thickness and Refractive Index in One Measurement of Phase-Modulated Ellipsometry. *J. Opt. Soc. Am. A* **2006**, *23*, 2639–2644.